engineering proceedings

MDPI

Proceeding Paper

The IMU Sensor for In-Situ 3D Movement Monitoring of Particulate Matter †

Barbora Černilová * and Jiří Kuře

Department of Electrical Engineering and Automation, Faculty of Engineering, Czech University of Life Sciences Prague, Kamycka 129, 6-Suchdol, 165 00 Prague, Czech Republic; kure@tf.czu

* Correspondence: cernilova@tf.czu.cz

† Presented at The 11th International Electronic Conference on Sensors and Applications (ECSA-11), 26–28 November 2024; Available online: https://sciforum.net/event/ecsa-11.

Abstract: The contribution describes the prototype of a compact IMU sensor with dimensions of 30 × 20 × 10 mm. The sensor integrates a 3-axis gyroscope module, LSM6DSL, along with onboard memory and a processing unit. The device was used to measure linear motion along the x-axis over a distance of 630 mm, giving a measured length of 659 mm. The absolute error was 29 mm, with a relative error of 4.6%. This error is likely attributable to manual movement during the measurement process.

Keywords: the IMU sensor; movement monitoring; accelerometer; gyroscope; precise agriculture

1. Introduction

The object movement monitoring in three-dimensional space in agriculture allows for adaptation to current needs or planned implementation as a result of predictive analysis. The 3D movement monitoring has the potential for particulate matter movement analysis during handling and processing [1]. The inertial measurement units (IMU) are versatile instruments designed to measure both static gravitational acceleration and dynamic processes such as movement, shocks, and vibrations [2,3]. These capabilities make them effective tools for tracking soil motion and other environmental monitoring tasks with applications to livestock production as well [4]. In the agricultural, accelerometers are frequently employed for measuring vibrations by positioning them either on or beneath the surface of soil that is subject to mechanical stresses from agricultural machinery [5]. These vibrations, caused by dynamic mechanical loads, provide critical information for optimizing equipment operation and reducing soil compaction. By monitoring soil vibrations, accelerometers aid in preventing soil degradation, which is crucial for maintaining long-term soil health [6]. The integration of accelerometers within precision agriculture is now a critical aspect of modern farming practices. These sensors, which measure both static and dynamic forces, play a pivotal role in evaluating the mechanical impacts of machinery on soil [7,8]. In precision agriculture, accelerometers are integrated with broader technologies, including Geographic Information Systems (GIS) and Global Navigation Satellite Systems (GNSS), to create comprehensive platforms for monitoring soil conditions and optimizing machinery performance. Beyond these applications, the IMU sensors have been employed to monitor large-scale soil movements, such as landslides. For instance, Kaharuddin et al. (2022) [9] demonstrated their utility as inclinometers for detecting landslides. However, their findings indicated that accelerometers may suffer from significant interference, rendering them less suitable for applications requiring high precision. This issue can, however, be addressed through the implementation of advanced filtering algorithms such as the Kalman filter, which is effective in mitigating noise and sensor bias [10,11]. In addition to the Kalman filter, numerous other filters can be applied,

Citation: Černilová, B.; Kuře, J. The IMU Sensor for In-Situ 3D Movement Monitoring of Particulate Matter. *Eng. Proc.* **2024**, *6*, x. https://doi.org/10.3390/xxxxx

Academic Editor(s):

Published: 26 November 2024

such as the Complementary filter, Butterworth filter, Savitzky-Golay filter, and Wavelet filter [12–15]. The use of such filters enhances the accuracy of accelerometers in environmental monitoring tasks, ensuring more reliable data collection.

The objective of this paper was to present a prototype device consisting of an accelerometer and gyroscope designed for tracing the movement of particulate materials. The primary advantage of this device lies in its compact dimensions, which enable it to adapt seamlessly to the flow of particulate substances. This adaptability ensures that the device can effectively capture the dynamics of particle movement, offering enhanced precision in tracking and monitoring within diverse particulate systems. However, this presents a significant challenge in developing a compact, cost-effective device that integrates only an accelerometer and gyroscope, capable of tracking particulate matter in situ [8,15,16].

2. Materials and Methods

2.1. Module Assembly

In this contribution, a prototype IMU sensor is presented, which consists of a 3-axis gyroscope and accelerometer module LSM6DSL, internal memory and a processing unit, which allow it to accurately monitor and record changes in the movement of particles during movement continuously. The LSM6DSL is an integrated MEMS sensor combining both an accelerometer and a gyroscope, thus enabling six-axis motion sensing. The accelerometer offers measurement ranges between ±2 g and ±16 g, while the gyroscope provides measurement ranges between ±125 dps and ±2000 dps. Acceleration was measured and recorded in units of g, where 1 g is equivalent to 9.81 m/s². The gyroscope data was captured in degrees per second (°/s).

The prototype module was designed with compact dimensions of 35 × 20 × 10 mm, including the protective casing. The size of the die itself is 20 × 20 mm. The casing was made of ABS material. The wired prototype connects to a computer via USB, enabling real-time data acquisition and immediate analysis. The USB connection serves both as a data transmission interface and a power supply for the module. The completed IMU sensor prototype is shown in the Figure 1a. As can be observed from the figure, colored wiring extends from the device, allowing for additional programming of the module. The Figure 1b presents the sensor with the axes marked in the X, Y, and Z directions.

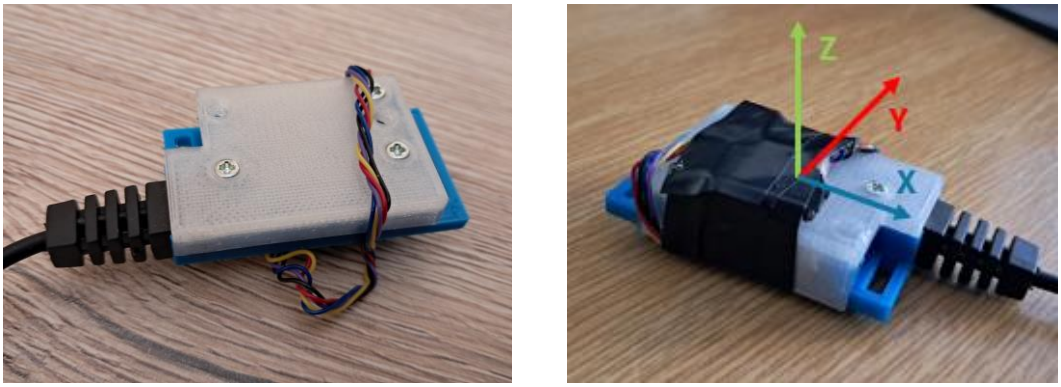

(**a**) (**b**)

Figure 1. Prototype inertial measurement units of the sensor, which is stored in a package with handles for possible fixing (**a**) and the sensor with axes marked in the X, Y and Z directions (**b**).

2.2. The Software

The software application was used for data reading and storage, specifically designed to interact with the LSM6DSL sensor. This software allowed users to select the measurement ranges for both the accelerometer and the gyroscope. For the accelerometer, the selectable ranges were between ±2 g and ±16 g, while for the gyroscope, the ranges varied from ±125 dps to ±2000 dps. Furthermore, the software enabled users to configure the data

storage size, which could range from 500 to 5000 data points per file. It also provided the option to toggle the gyroscope on or off, as well as the capability to visually display the currently measured data, as evident in the Figure 2. The visualized data consists of six curves, with the blue curve representing the X-axis, the green curve the Y-axis, and the red curve the Z-axis. The gyroscope data is displayed as bold curves, while the accelerometer data is shown as thin curves. The image clearly depicts the motion of the module along the X-axis. The trajectory indicates an almost linear movement, corresponding to a manual displacement in the direction of the X-axis. However, minor deviations are observed in the Y and Z axes, indicating slight motion in those directions as well. Additionally, the data reveals a subtle rotation during the movement, evidenced by the slight shifts in the gyroscope curves. The Figure 3 shows the user interface, which enables the required configuration.

The data is saved in a text file after reading. The first row contains the column headers, identifying the respective data fields. Subsequent rows represent the recorded data, with each row corresponding to a single sample. The first three columns contain data from the accelerometer along the X, Y, and Z axes. The following three columns contain data from the gyroscope, also in the X, Y, and Z axes.

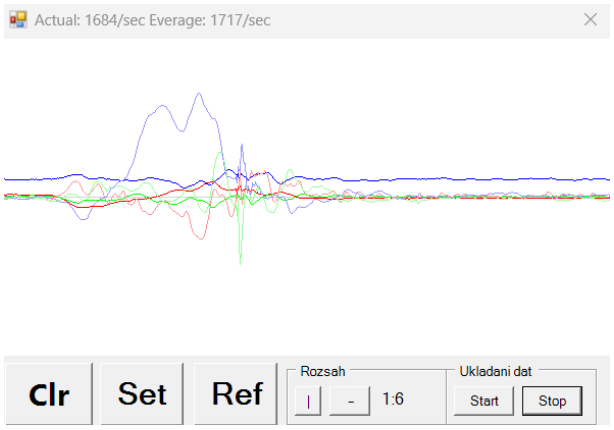

Figure 2. The visualization of the currently measured data from the software used.

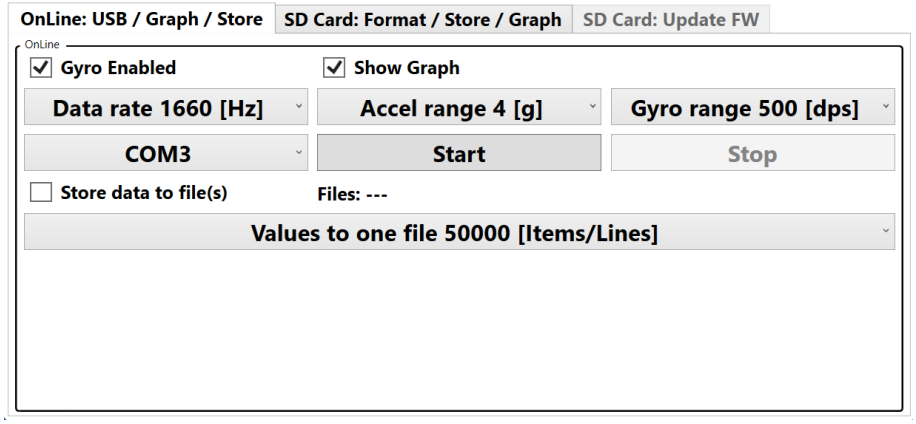

Figure 3. The user interface of the software that allows the required measurement settings.

2.3. The Experiment

The experiment was conducted by mounting the IMU sensor onto a frame within a laboratory soil box. The mounting on the frame of the soil box is shown in Figure 4. From the image, it is evident that the device was positioned to measure along the X-axis due to its attachment. The frame allowed for linear movement, enabling a controlled linear displacement of the device in the desired direction. Measurements were taken along the X-

axis during linear movement, with the accelerometer oriented towards the -X direction. The displacement was manually executed over a distance of 630 mm.

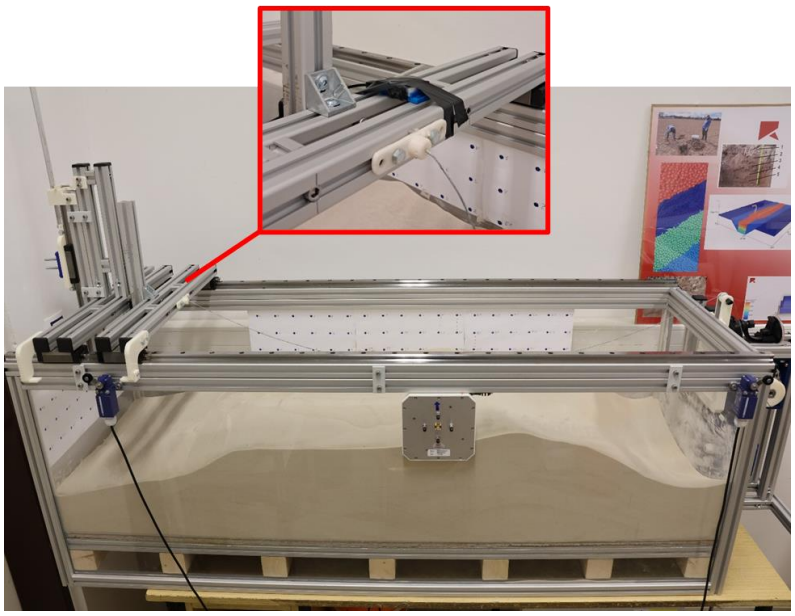

Figure 4. The laboratory soil box and the mounting of the device on the frame of the box.

3. Results

Measurements were taken along the X-axis during linear motion, with the accelerometer oriented in the -X direction. Figure 5 presents the accelerometer data specifically along the X-axis. The data show the presence of noise and spikes, with the actual movement lasting approximately 1.15 s.

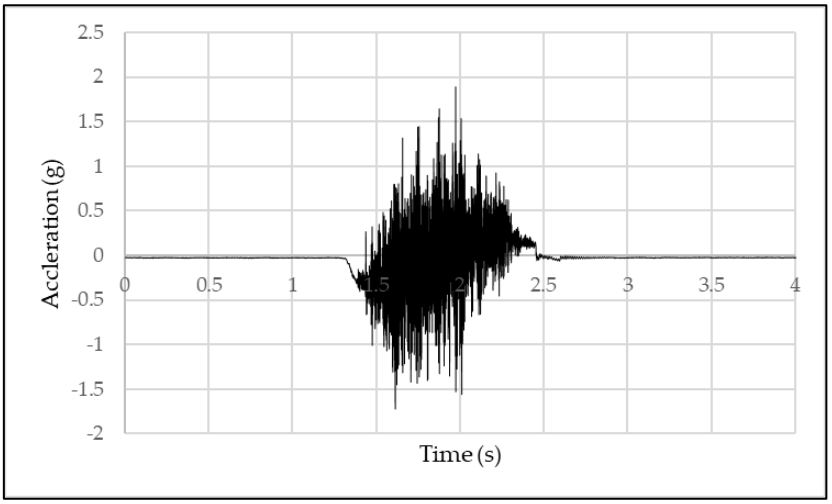

Figure 5. A graph showing the raw data obtained from the accelerometer in the X-axis.

To mitigate the noise and enhance the accuracy of the recorded data, a Kalman filter was applied to the measurements, as illustrated in Figure 6. The raw data were then converted from units of g to acceleration in m/s² using Equation (1).

$$a_i = ag_i * 9.81 \quad (1)$$

where:

a_i represents the acceleration in a given step (m/s²);
ag_i is the acceleration in the given step (g);

1 g = 9.81 m/s².

The correction was also applied to the raw data to obtain more accurate results. From the graph in Figure 6, it can be observed that the maximum acceleration value from the measured data was recorded as 0.3249 m/s². The graph further shows a negative progression, which was caused by the device being oriented along the negative X-axis during measurement.

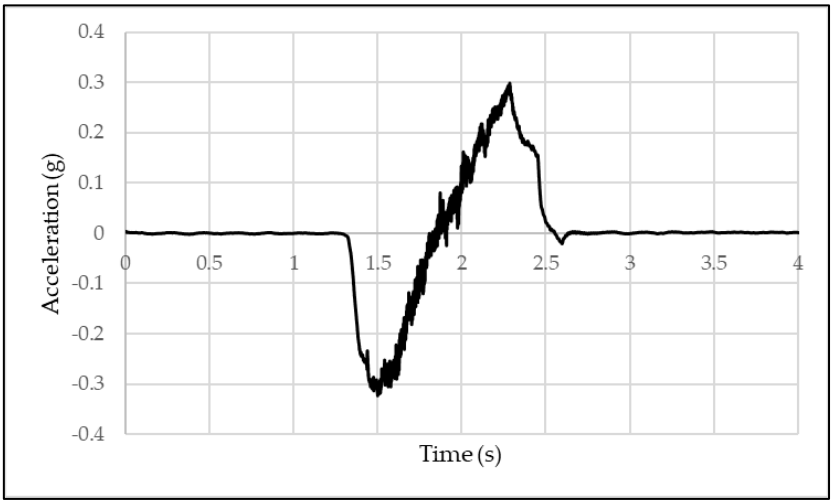

Figure 6. A graph showing the adjusted data to which a Kalman filter has been applied with an apparent time course of acceleration.

Furthermore, the acceleration was converted to velocity. The calculation of velocity is based on the integration of acceleration over time. In discrete form, the velocity (v_i) at a specific time step can be calculated using the following formula:

$$v_i = a_i * (t_i - t_{i-1}) + v_{i-1} \quad (2)$$

where:

v_i is the velocity at the current time step (m/s),
a_i is the acceleration at the current time step (m/s²),
t_i is the current time (s),
t_{i-1} is the time from the previous time step (in s),
$(t_i - t_{i-1})$ represents the time interval between two measurements (s),
v_{i-1} is the velocity from the previous time step (m/s).

The recalculation allows for the determination of the instantaneous velocity over time, which is shown in Figure 7. It is shown in the graph that the highest speed achieved was 0.9696 m/s.

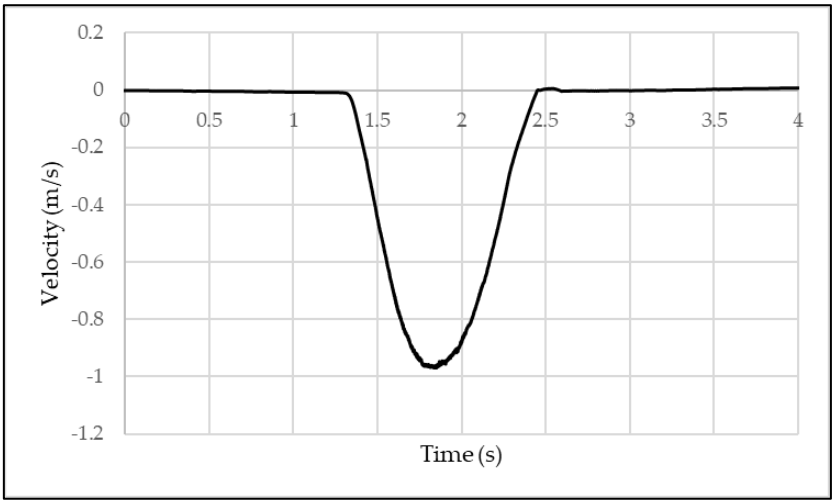

Figure 8. A graph iustrating the values converted from acceleration to velocity with a maximum velocity value of 0.9696 m/s.

Finally, the velocity was recalculated to determine the displacement. The distance s can be calculated as the integral of velocity v over time t. In discrete form, for individual time steps, the distance can be calculated using the equation:

$$s_i = v_i * (t_i - t_{i-1}) + s_{i-1} \quad (3)$$

where:

s_i is the distance at the current time step (m),
v_i is the velocity at the current time step (m/s),
t_i is the time at the current time step (s),
t_{i-1} is the time from the previous time step (s),
$(t_i - t_{i-1})$ is the time interval between two measurements (s),
s_{i-1} is the distance from the previous time step (m).

From this recalculation, the instantaneous displacement over time can be determined, as shown in Figure 9.

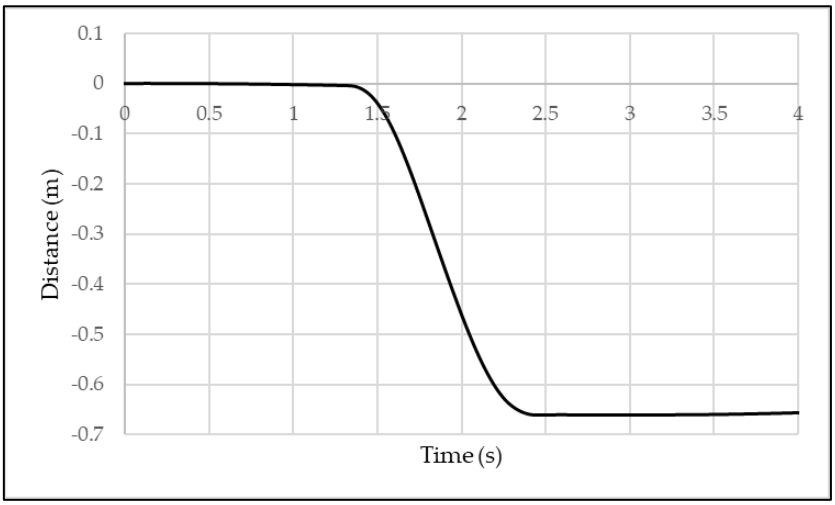

Figure 10. A graph showing the resulting values of the distance over time that was calculated by integrating the velocity.

According to the measurement, the total distance was found to be 659 mm. However, this result could have been influenced by several factors, such as inaccuracies in the accelerometer, misalignment in the axis, noise errors, filtering inaccuracies, or errors

during manual movement along the 630 mm distance. According to Equation (4), the relative error was calculated, while Equation 5 was used to determine the absolute error. The absolute error value was 29 mm and the relative error value was 4.6%.

$$Absolute\ error = \ Measured\ value - True\ value = 659\ \text{mm} - 630\ \text{mm} = 29\ \text{mm} \quad (4)$$

$$Relative\ error = \frac{Absolute\ error}{True\ value} = \frac{29\ \text{mm}}{630\ \text{mm}} = 4.6\% \quad (5)$$

4. Discussion and Conclusions

Our research employed an Inertial Measurement Unit (IMU) sensor for in-situ 3D tracking of particulate matter, that has potential to capture detailed movement patterns and enhance our understanding of particle dynamics during the particulate matter interactions with agricultural tools [16]. The sensor utilizes 3-axis gyroscope module LSM6DSL, internal memory and processor unit, allowing it to accurately monitor and record changes in particulate matter movement continuously during the motion. The objective of this paper was to develop a cost-effective smart sensor, aimed at providing a practical and economical solution for real-time data acquisition. The prototype introduced in this study is based on a USB interface. Looking ahead, future iterations of this sensor will be designed around a battery-powered concept. The shift to a battery-based prototype has potential for real-time, in-field data collection, offering better understanding of agricultural processes.

The assembly requirement aimed to achieve optimal dimensions to minimize disturbance to particle flow. The proposed module including housing features extremely compact dimensions of 30 × 20 × 10 mm. The compactness of the module allows it to integrate seamlessly into the flow of particles, ensuring minimal disruption to the natural dynamics of particulate systems. Currently, the IMU sensor is designed in a rectangular cuboid shape. However, the next prototype will feature a spherical design. This change in shape is aimed at improving the sensor's adaptability and interaction with the surrounding environment.

The IMU sensor was used to measure linear motion along the x-axis over a distance of 630 mm. The measured length was 659 mm, resulting in an absolute error of 29 mm and a relative error of 4.6%. However, this result may have been influenced by several factors, including inaccuracies in the accelerometer, misalignment of the axis, noise errors, filtering inaccuracies, or manual movement errors during the 630 mm distance. The primary cause of the discrepancy is likely the manual handling during the measurement. These findings suggest that minimizing human-induced factors could improve measurement accuracy in future tests.

Author Contributions: Conceptualization, B.Č. and J.K.; methodology, J.K.; validation, J.K.; formal analysis, B.Č.; investigation, J.K.; resources, B.Č. and J.K.; data curation, J.K.; writing—original draft preparation, B.Č.; writing—review and editing, J.K; visualization, B.Č.; supervision, J.K.; project administration, B.Č.; funding acquisition, B.Č. All authors have read and agreed to the published version of the manuscript.

Funding: This research was funded by internal grant agency of Faculty of Engineering, grant number 2024:31200/1312/3101, grant title: "Verification of the particles motion within a simulation model based on the Discrete Element Method, employing a module equipped with an accelerometer".

Institutional Review Board Statement: Not applicable.

Informed Consent Statement: Not applicable.

Data Availability Statement: The data presented in this study are available by reasonable request from the corresponding author.

Acknowledgments: We would like to express our sincere gratitude to Ing. Pavel Děd, and Ing. Petr Novák, for their collaboration, particularly in relation to the development of the device and the software for data acquisition.

Conflicts of Interest: The authors declare no conflict of interest. The funders had no role in the design of the study; in the collection, analyses, or interpretation of data; in the writing of the manuscript; or in the decision to publish the results.

References

1. Ariza-Sentís, M.; Vélez, S.; Martínez-Peña, R.; Baja, H.; Valente, J. Object detection and tracking in Precision Farming: A systematic review. *Comput. Electron. Agric.* **2024**, *219*, 108757. https://doi.org/10.1016/j.compag.2024.108757.
2. Ooi, G.L.; Wang, Y.H. Applying MEMS Accelerometers to Measure Ground Vibration and Characterize Landslide Initiation Features in Laboratory Flume Test. In Proceedings of the Geo-Congress 2014, Atlanta, Georgia, 23–26 February 2014; pp. 2019–2028. https://doi.org/10.1061/9780784413272.197.
3. Zhang, D.; Liu, C.; Nguyen, B.K. Low-Cost Real-Time Localisation for Agricultural Robots in Unstructured Farm Environments. *Machines* **2024**, *12*, 612. https://doi.org/10.3390/MACHINES12090612.
4. Hu, S.; Reverter, A.; Arablouei, R.; Bishop-Hurley, G.; McNally, J.; Alvarenga, F.; Ingham, A. Analyzing Cattle Activity Patterns with Ear Tag Accelerometer Data. *Animals* **2024**, *14*, 301. https://doi.org/10.3390/ANI14020301.
5. Singh, A.; Nawayseh, N.; Samuel, S.; Dhabi, Y.K.; Singh, H. Real-time vibration monitoring and analysis of agricultural tractor drivers using an IoT-based system. *J. Field Robot.* **2023**, *40*, 1723–1738. https://doi.org/10.1002/rob.22206.
6. Kusumawardani, R.; Nugroho, U.; Fansuri, M.H.; Mindiastiwi, T.; Yuniarti, W.; Hilmi, A.S. The impact of vehicle load inducing vibrations on the subgrade soil particle acceleration. *J. Eng. Sci. Technol.* **2018**, *13*, 1440–1450.
7. Justa, J.; Šmídl, V.; Hamáček, A. Fast AHRS Filter for Accelerometer, Magnetometer, and Gyroscope Combination with Separated Sensor Corrections. *Sensors* **2020**, *20*, 3824. https://doi.org/10.3390/S20143824.
8. Shaheb, M.R.; Sarker, A.; Shearer, S.A.; Shaheb, M.R.; Sarker, A.; Shearer, S.A. Precision Agriculture for Sustainable Soil and Crop Management. In *Soil Science—Emerging Technologies, Global Perspectives and Applications*; InTech Open: Rijeka, Croatia, 2022. https://doi.org/10.5772/INTECHOPEN.101759.
9. Kaharuddin, S.; Ain, M.F.; Mamat, M.N.; Abdullah, M.N.; Yusob, M.F.B.M. Soil mass movement monitoring for landslide detection using low-cost accelerometer sensor as inclinometer. *J. Phys. Conf. Ser.* **2022**, *2312*, 012056. https://doi.org/10.1088/1742-6596/2312/1/012056.
10. Rossi, Y.; Tatsis, K.; Awadaljeed, M.; Arbogast, K.; Chatzi, E.; Rothacher, M.; Clinton, J. Kalman filter-based fusion of collocated acceleration, gnss and rotation data for 6c motion tracking. *Sensors* **2021**, *21*, 1543. https://doi.org/10.3390/s21041543.
11. Saho, K. Kalman Filter for Moving Object Tracking: Performance Analysis and Filter Design. In *Kalman Filters—Theory for Advanced Applications*; IntechOpen: Rijeka, Croatia, 2018. https://doi.org/10.5772/intechopen.71731.
12. Rzucidło, P.; Kopecki, G.; Szczerba, P.; Szwed, P. Analysis of Stochastic Properties of MEMS Accelerometers and Gyroscopes Used in the Miniature Flight Data Recorder. *Appl. Sci.* **2024**, *14*, 1121. https://doi.org/10.3390/APP14031121.
13. El Dahr, R.; Lignos, X.; Papavieros, S.; Vayas, I. Dynamic Assessment of the Structural Behavior of a Pedestrian Bridge Aiming to Characterize and Evaluate Its Comfort Level. *Buildings* **2023**, *13*, 3053. https://doi.org/10.3390/BUILDINGS13123053/S1.
14. Tahir, S.B.U.D.; Jalal, A.; Kim, K. Wearable Inertial Sensors for Daily Activity Analysis Based on Adam Optimization and the Maximum Entropy Markov Model. *Entropy* **2020**, *22*, 579. https://doi.org/10.3390/E22050579.
15. Tereshkov, V.M. A Simple Observer for Gyro and Accelerometer Biases in Land Navigation Systems. *J. Navig.* **2015**, *68*, 635–645. https://doi.org/10.1017/s0373463315000016.
16. Pásthy, L.; Szabó, B.; Tamás, K. Measuring and modelling of soil displacement from a horizontal penetrometer and a sweep using an IMU sensor fusion and DEM. *Soil Tillage Res.* **2024**, *244*, 106207. https://doi.org/10.1016/J.STILL.2024.106207.